Limits on the excitable behavior of a semiconductor laser with optical feedback

Jorge Manuel Méndez,* J. Aliaga,† and G. B. Mindlin‡
Departamento de Física "J.J. Giambiagi," Facultad de Ciencias Exactas y Naturales, U.B.A., Ciudad Universitaria, Pabellón I, 1428 Buenos Aires, Argentina
(Received 10 August 2004; published 25 February 2005)

Recently, it was proposed that semiconductor lasers with optical feedback present a complex behavior that can be described as noise driven excitable. In this work we investigate in which region of parameter space this description is adequate. We conclude that the region of the parameter space in which the system displays noise driven excitable behavior is a subset of the region in which presents low frequency fluctuations.

DOI: 10.1103/PhysRevE.71.026231 PACS number(s): 05.45.−a, 42.60.Mi, 42.65.Sf

I. INTRODUCTION

The dynamics of semiconductor lasers with optical feedback has been intensively studied since 1977 [1]. One particularly interesting behavior shown by the laser is the low frequency fluctuations regime (LFF). It is characterized by the existence of irregularly occurring high intensity fluctuations on microsecond scales which are longer than the other time scales of the semiconductor dynamics, like the period of the relaxation oscillations or the round trip time of the external cavity (hence the name LFF) [2]. The LFF regime has been extensively studied. It was intensively debated whether this dynamics is the result of noise driven excitability or if its complex dynamics is high dimensional chaos [2,3]. The most widely studied model is the Lang and Kobayashi one (LK), which presents both high dimensional chaos [4,5] and excitability [6]. This model is obtained taking into account a single mode laser operating with weak feedback level. On the other hand there is strong experimental evidence of multimode dynamics of semiconductor lasers with optical feedback [7,8]. Recently, several steps have been taken in order to build up confidence in the noise driven scenario [2,9–15]. In particular, a dynamical model to characterize the excitable behavior of the semiconductor laser with optical feedback has been proposed by Eguia *et al.* [9].

An excitable system is one that possesses a stable stationary state and has a threshold for an external perturbation [16]. If the perturbation is smaller than the threshold, the trajectory will return to the stationary state performing a short excursion in its physical variables. Otherwise, if the perturbation is larger than the threshold, the trajectory returns to the stationary state making a large excursion in the phase space called pulse. When the perturbation overcomes the threshold, the amplitude of the pulses becomes independent of the perturbation amplitude. The direct test for excitability consists in verifying the existence of this threshold in the response of the system when a perturbation is applied. An important characteristic of an excitable system is the existence of a refractory time. While the system is performing an excitable pulse, it does not response to other perturbations. Another indirect test consists in the analysis of the dynamics under the forcing of one of its parameters.

Excitability was experimentally found in semiconductor lasers with optical feedback [2], solid state lasers with an intracavity saturable absorber [17], distributed feedback semiconductor lasers [18], and semiconductor optical amplifiers [19]. In particular, for the case of the solid state laser with intracavity saturable absorber direct tests have been especially clear to uncover the excitable behavior [17]. One of the motivations behind the search for excitability in optical systems comes from the unique computational properties shown by natural excitable systems like neurons [20,21] and from the possibility to make optical networks using these properties [22].

When the dynamics of the excitable system is strongly influenced by noise, it is useful either to compute the interevent time distribution or other statistics quantifiers as the parameters are varied. In Ref. [10] this analysis has been performed for the semiconductor laser with optical feedback, in which the effect of the intrinsic noise had to be taken into consideration. This study [10] has been done in a particular condition and does not represent all the experimental regimes shown by the experiment.

Although excitability in semiconductor lasers with optical feedback has been experimentally identified, no precise limitations within the LFF behavior have been investigated [2]. In this work we report that not all the LFF patterns of behavior are consistent with noise-driven excitable dynamics. We will clarify the influence that the maximum gain mode (MGM) has on the excitable scenario, and we will analyze the compatibility between the experimental excitability and the one displayed by the dynamical model of Eguia *et al.* [9].

This paper is organized as follows. Section II describes the results of the statistics quantifiers for the noisy dynamics of the theoretical model to be compared with the experimental results. Section III contains the experimental results regarding the limits on the excitable behavior. In Sec. IV we present the conclusions of the work.

II. NOISY DYNAMICS OF THE DYNAMICAL MODEL: STATISTICAL STUDY

In Ref. [9] Eguia *et al.* proposed a dynamical model to explore the statistics of noise driven excitable systems, in

*Electronic address: jmendez@df.uba.ar
†Electronic address: jaliaga@df.uba.ar
‡Electronic address: gabo@df.uba.ar

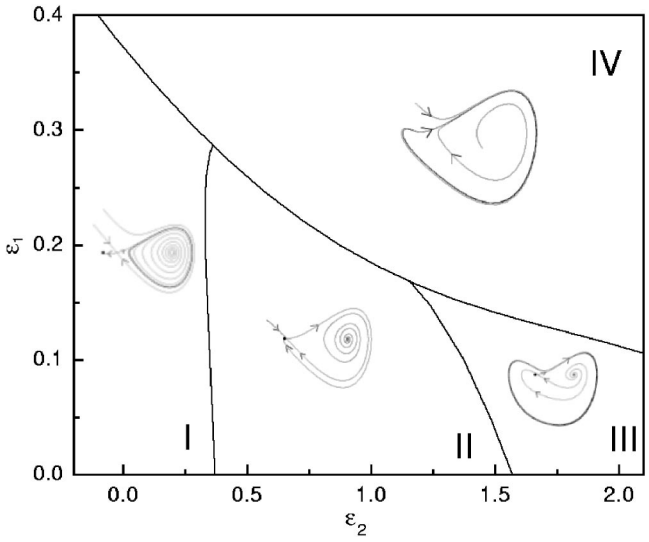

FIG. 1. Bifurcation diagram and phase portrait for the dynamical model. Regions I, II, and III have three fixed points. Regions I and III are bistable, region II is excitable, and region IV is oscillatory.

order to compare it with the interspike distribution of the LFF regime displayed by semiconductor lasers with optical feedback. A complete understanding of the dynamical model can be seen in Ref. [9]. The system of equations of this model reads

$$x' = y, \tag{1}$$

$$y' = x - y - x^3 + xy + \epsilon_1 + \epsilon_2 x^2, \tag{2}$$

with $(x,y) \in \mathbb{R}^2$, and $\epsilon_1, \epsilon_2 \in \mathbb{R}^+$. The noisy dynamics is studied adding in the y component a white Gaussian noise with zero mean and variance D. Qualitatively the model displays four different regions on the parameter plane (ϵ_1, ϵ_2) separated by global bifurcations (Fig. 1). Two of the previously mentioned regions are bistable (region I and III), one is excitable (region II), and the other is oscillatory (region IV). In the excitable region there are three fixed points: a stable node, a saddle point, and a repulsor. The transitions from region I to region II, and from region II to region III are saddle-loop global bifurcations, whereas the transition from any region to region IV is an Andronov bifurcation. The bistable regions have a stable node, a saddle point, a repulsor, and a limit cycle. In the case of region I it is an small limit cycle and in region III a large one which encompasses the whole dynamics.

In Fig. 2 we show the probability distributions of interdropout events (P) and maps of the minimum point of return between two dropouts (V_{ret}) versus their time interval (ISI) for different values of the ϵ_2 parameter in region I and II. The ϵ_1 parameter is varied in order to explore the transition to region IV. As previously stated in Ref. [10], there are two characteristic times in P, more easily recognized in the vicinity of the codimension 2 bifurcation point [$\epsilon_2 = 0.5$, Fig.

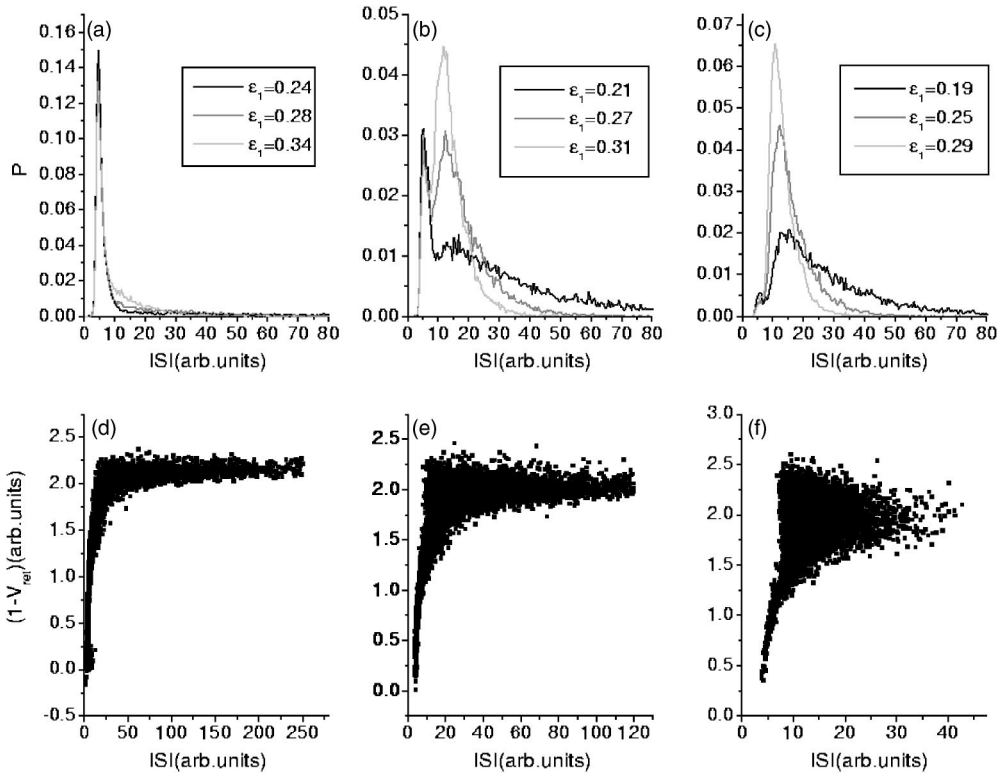

FIG. 2. Analysis of the noisy dynamics of the model. Probability distribution of interdropout events (P) for (a) $\epsilon_2 = 0.2$, (b) $\epsilon_2 = 0.5$, and (c) $\epsilon_2 = 0.7$. In each figure we show P for several values of the parameter ϵ_1 as is indicated in the insets. Map of the minimum point of return between two dropouts (V_{ret}) versus the time interval between them (ISI): (d) $(\epsilon_1, \epsilon_2) = (0.24, 0.2)$, (e) $(\epsilon_1, \epsilon_2) = (0.21, 0.5)$, and (f) $(\epsilon_1, \epsilon_2) = (0.19, 0.7)$.

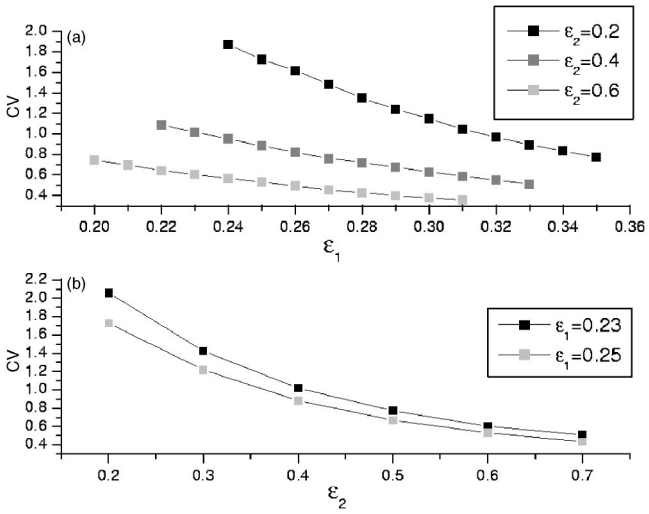

FIG. 3. Analysis of the noisy dynamics of the model. (a) Coefficient of variation (CV) versus ϵ_1 for several values of ϵ_2 indicated in the inset. (b) The same as (a) exchanging parameters ϵ_1 and ϵ_2.

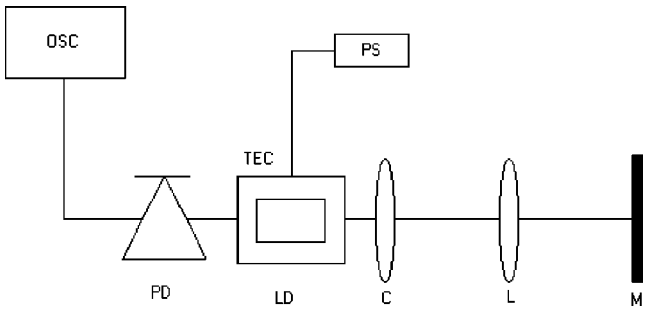

FIG. 4. Experimental setup: LD, laser diode; PD, photodiode; OSC, oscilloscope; C, collimator; L, lens; M, mirror; TEC thermoelectric cooler; PS power source.

2(b)]. These two characteristic times owe their existence to the anticipation of each of the two bifurcations. The left peak of P corresponds to the saddle-loop bifurcation, and the other peak to the Andronov bifurcation, which gives a distribution with a Kramers-like tail [23]. When the ϵ_2 parameter is driven inside region I, the two characteristic times tend to be more separated [ϵ_2=0.2, Fig. 2(a)]. Otherwise, the removal of the ϵ_2 parameter from the vicinity of the codimension-2 bifurcation point in the other direction drives it to a situation similar to a one dimensional system which corresponds to the infinite dissipation limit of the excitable system [24] [ϵ_2=0.7, Fig. 2(c)]. In this case, only a small fraction of the events comes from the anticipation of the saddle-loop bifurcation.

Another way to distinguish these two different sorts of events which produce the two characteristic times is to analyze the map of the V_{ret} vs ISI. The events that spring from the "infinite dissipation" distribution are essentially renewal ones and they must complete the relaxation to the attractor or pass near it before executing a new dropout. These events are recognized on the map as the ones that are located on the horizontal strip [Figs. 2(d)–2(f)]. The events which cause the left peak in P are translated on this map as a vertical strip

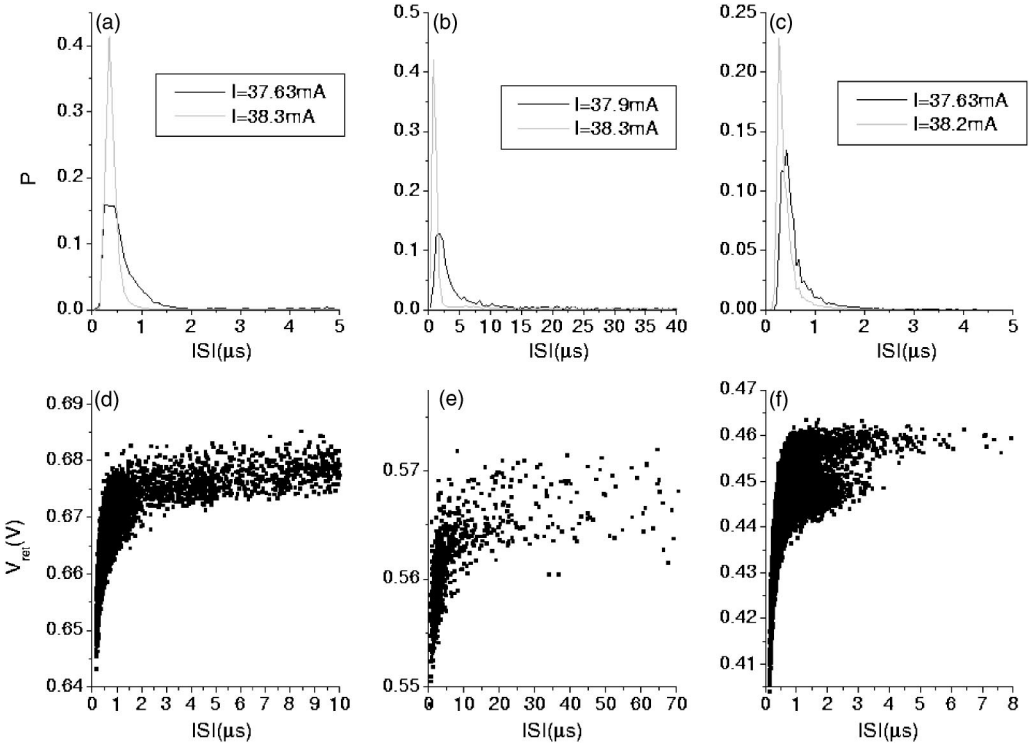

FIG. 5. Experimental dynamics influenced by the MGM: Probability distributions of interdropout events (P) for different threshold reductions (a) ξ=11%, (b) ξ=8.6%, and (c) ξ=6.8%. In each figure we show P for several values of pumping current (I) as is indicated in the insets. Map of the maximum point of return between two dropouts (V_{ret}) versus the time interval between them (ISI) for different threshold reductions: (d) ξ=11% and I=37.63 mA, (e) ξ=8.6% and I=37.9 mA, and (f) ξ=6.8% and I=38.2 mA.

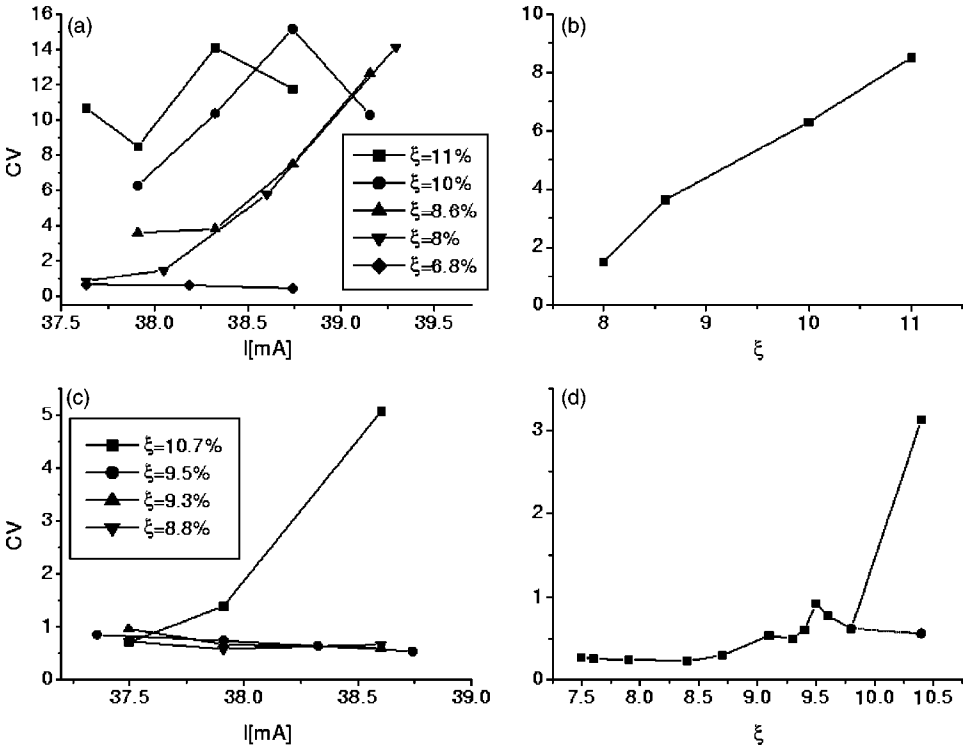

FIG. 6. Coefficient of variation (CV) for several experimental conditions. (a) CV versus pumping current (I) for several values of threshold reduction (ξ) indicated in the inset (for the case III A). (b) CV versus threshold reduction for a constant pumping current (for case III A). (c) CV versus pumping current for several values of threshold reduction indicated in the inset (for the case III B). (d) Detailed analysis of CV versus threshold reduction for a constant pumping current (for case III B). The points connected by the dotted line represent the dynamics without taking into consideration the MGM.

with a very coherent ISI between the dropouts because they come from a noise-induced or deterministic limit cycle.

When the dynamics of a system consists of a competition between two very different time scales, like in region I, it is useful to consider the coefficient of variation (CV), which is the standard deviation divided by the mean of the time interval between spikes [25,26], and explore their dependence with the parameters. In Fig. 3(a) the results of sweeping ϵ_1 parameter are shown, whereas the results of sweeping ϵ_2 parameter are displayed in Fig. 3(b). It is worth noting that CV is monotonically decreasing with ϵ_1 [Fig. 3(a)] and ϵ_2 [Fig. 3(b)].

These statistical quantifiers of the dropout or spike train and the map of V_{ret} vs ISI have been calculated in order to distinguish whether a case is excitable or not. In particular, an experimental condition would be considered as excitable when the values and dependencies of these quantifiers and maps are equivalent to those in the dynamical model.

III. REGIONS OF PARAMETER SPACE

The experimental setup is shown in Fig. 4. The semiconductor laser used is the single transverse mode Sharp LTO30MD/MF, emitting with a nominal wavelength of 750 nm. The solitary laser threshold is 36.66 mA. The laser is thermally stabilized up to 0.01 C. A mirror of high reflectivity (>90%) is placed in front of the laser beam, in order to return part of the light emitted into the laser. The mirror is placed at 45 cm from the laser edge. A collimator and an AR-coated lens are placed into the cavity to reduce the beam divergence and to mode match the returned beam with the emitted beam. The intensity output is detected by a 1-GHz bandwidth photodiode and the signal is analyzed with a Tektronix TDS5052 500-MHz oscilloscope. The amount of feedback is controlled by the interposition of a neutral filter which allows a continuous attenuation in the laser beam (circular linear wedge neutral density filter: Melles Griot 03FDC003).

Broadly speaking, the dynamics of the semiconductor laser with optical feedback can be classified into three different regimes: stable intensity emission, LFF, and coherence collapse (ordered in ascending amount of pumping current). Also, in some circumstances the coexistence of stable emission of the MGM with the LFF emission has been observed [27]. The usual studies made to analyze excitability have avoided the MGM. In particular, Yacomotti *et al.* [10] have demonstrated that the variation of the interevent histogram caused by variations in the pumping current or the feedback level are equivalent to variations in each one of the parameters of the model proposed by Eguia *et al.* [9]. The experimental condition taken by Yacomotti *et al.* can be considered as an example of the ideal excitability displayed by this laser system. This situation was maintained in all their parameters exploration. If greater variations in the parameters are allowed, it will be clear that there exist limitations on the excitable behavior.

In order to delimit the excitable region, it is necessary to achieve both a detailed analysis of the dynamics within the LFF regime and an understanding of the dynamics displayed by the system with the influence of the MGM. To put forward the limitations on the excitability we will show the experimental results for two different alignments. In the first case (sec. III A), we have aligned the system to increase the probability of occurrence of the MGM (best alignment condition). Conversely in the second case (Sec. III B) we have intentionally damaged the alignment condition to get rid of the MGM as much as possible without deteriorating the feedback level.

A. Dynamics influenced by the MGM

We performed a sweep in the pumping current and feedback level to uncover whether the system with dynamics highly influenced by the MGM is excitable or not, and whether it is consistent with the dynamical model. The probability distribution of time between dropout events shows that the left peak (located in times less than 1 μs) increases when the current is increased [Figs. 5(a)–5(c)]. This peak corresponds to a burstinglike activity characterized by a well-defined frequency of oscillation. Furthermore, P presents contributions in the order of several microseconds that come from the highly stable MGM. Although the shape of the distributions is similar to the ones present in the dynamical model for the region I [Fig. 2(d)], their dependence on the pumping current is not the same as the dependence the model has on the ϵ_1 parameter (from the work of Yacomotti *et al.* it is expected that the dependence of P on the pumping current is equivalent to that on the ϵ_1 parameter). Moreover, it was experimentally verified that the tail extended on long times has an exponential dependency which is an indication that the fluctuations, which drive the laser intensity out of the MGM, are essentially created by an escape problem [29].

Another important issue is the existence of two strips on the map of V_{ret} vs ISI [Figs. 5(d)–5(f)]. For a threshold reduction of 11% the two strips are clearly distinguished, one is essentially horizontal and the other vertical [Fig. 5(d)]. In this case the shape of the map is similar to that of the model in region I (bistable), indicating that the dynamics might have the same topology in the phase space (a node, a saddle point, a repulsor, and a small limit cycle). When the feedback is reduced, the dynamics can no longer be separated into a bursting and stable state with very different characteristic times in each state [Fig. 5(f)]. The reduction of the feedback level has destabilized the MGM producing visits to it with smaller residence times [Figs. 5(c) and 5(f)]. Also, the map of V_{ret} vs ISI has lost its similarity to the maps observed in the model. In this map is recognized the existence of two different levels of stable emission from which a dropout can be performed [Fig. 5(f)].

The existence of two different dynamical scenarios can be recognized in CV [Fig. 6(a)]. For a high feedback level, CV is much greater than those observed in the dynamical model [Fig. 6(a) with $\xi=11\%$]. On the other hand, smaller feedback levels give values of CV like the one in the model [Fig. 6(a) with $\xi=6.8\%$]. In-between levels of feedback allow us to observe how the competition with the MGM produces the conversion of values of CV near 1 to much greater values as the current is increased [Fig. 6(a) with $\xi=8\%$]. In Fig. 7 we show that this change of CV is caused by the appearance of the MGM. This abrupt change can also be seen in the probability distribution of interdropout time as an increment in the probability of having bursting dynamics [Fig. 7(b)], and in the time series as a differentiation between the two different ways of emission: the bursting and stable mode [Fig. 7(c)]. Another important issue is that, globally, the behavior of CV versus the feedback level is not equivalent to that displayed in the model when the ϵ_2 parameter is varied [Fig. 6(b)].

In Fig. 8 we show embeddings of time series for different feedback levels. When the feedback is high, the topology of

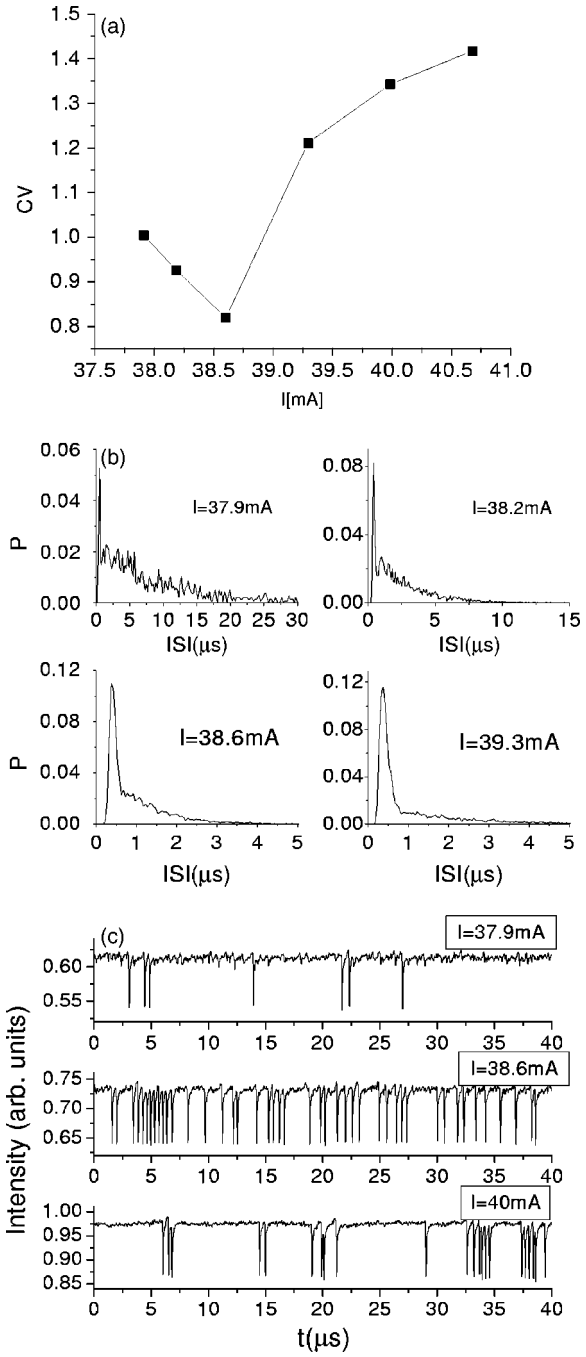

FIG. 7. Experimental transition from an usual excitable case to a case dominated by the MGM. (a) Coefficient of variation versus pumping current. (b) Probability distribution of interdropout times for a current sweep. (c) Time series for several pumping currents.

the phase space is compatible with having a stable node, a saddle point, a repulsor, and a small limit cycle with a well defined period of oscillation of 0.38 μs and a standard deviation of 0.12 μs [Figs. 8(a) and 8(b)]. As the feedback is decreased, it can be noticed that there are two different stationary states from which the dropouts can be performed [Figs. 8(c) and 8(d)]. These are the two levels previously observed in Fig. 5(f). One of these states is the MGM. The other one is a stable node (ESN: extended stable node) that can be identified with the stable node of the model based on

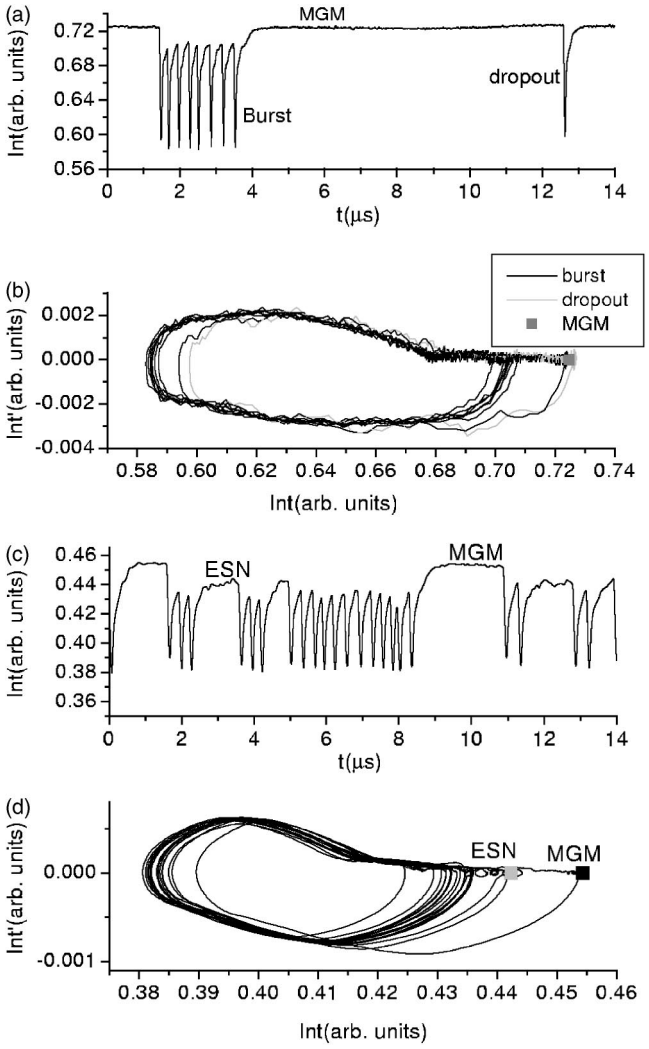

FIG. 8. Phase space reconstruction: (a) Segment of time series for pumping current $I=37.63$ mA and a threshold reduction of 10.6%. (b) Embedding of the time series of (a). (c) Segment of time series for pumping current $I=37.63$ mA and a threshold reduction of 6.8%. (d) Embedding of the time series of (c). MGM: maximum gain mode, ESN: excitable stable node.

the equivalence between the residence time in this node and the residence time in the stable node of an ideal experimental excitable case. For example, the average and the standard deviation of the residence time in the ESN for the case shown in Fig. 8(c) were computed to be approximately 1 and 0.6 μs, respectively. These values are similar to the ones computed for a case of ideal experimental excitability (Sec. III B with $I=37.5$ mA and with a threshold reduction of 8.8%) which are 1.3 and 0.8 μs. Also, to complete the similarity between the two cases, the average and the standard deviation of the clusters (consecutive dropouts events without a complete recovery up to the ESN level between them [10]) can also be computed yielding similar results (average 0.44 μs and standard deviation 0.15 μs for the first case and 0.48 and 0.3 μs for the second case used for the comparison). This last dynamical picture of low feedback is compatible to the dynamical model with the exception of the MGM. Furthermore, the probability to visit the MGM is much smaller

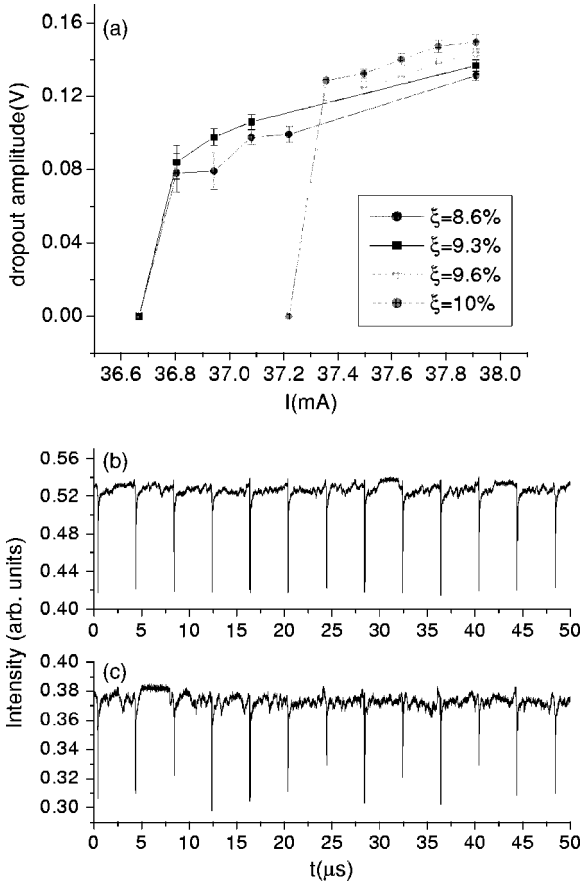

FIG. 9. (a) Average value and standard deviation of the dropouts amplitude as a function of the pumping current when the LFF appears for the case in which the dynamics is dominated by the MGM. (b) Time series of the laser intensity at the pumping current in which the dropouts appear for a threshold reduction of $\xi=9.6\%$ and (c) same as (b) but with $\xi=8.6\%$. In (b) and (c) several time series with one dropout event have been put one after the other to display orderly a group of events.

than in the previous cases with higher feedback.

In Fig. 9 we display the dropout amplitude as a function of the pumping current. The average amplitude of the dropout events is affected by a variation on the feedback level and a sharp transition related to the destabilization of the MGM is observed. This transition appears because the reduction of feedback causes the MGM to lose stability and the dropouts to be fired preferentially from the lower level. The destabilization of the MGM not only affects the current in which the dropouts appear but it also produces an increase of the variability in the dropout amplitude. In order to obtain CV values near the ones present in the model [Fig. 6(a)], it was necessary to reduce the feedback up to $\xi=8.6\%$. But at this level the possibility of defining a typical dropout event is seriously deteriorated [Fig. 9(c)].

B. Destabilization of the MGM

Empirically, we noticed that a slight deterioration of the alignment quality has a detrimental effect on the stability of the MGM. So, the system is intentionally taken out of the

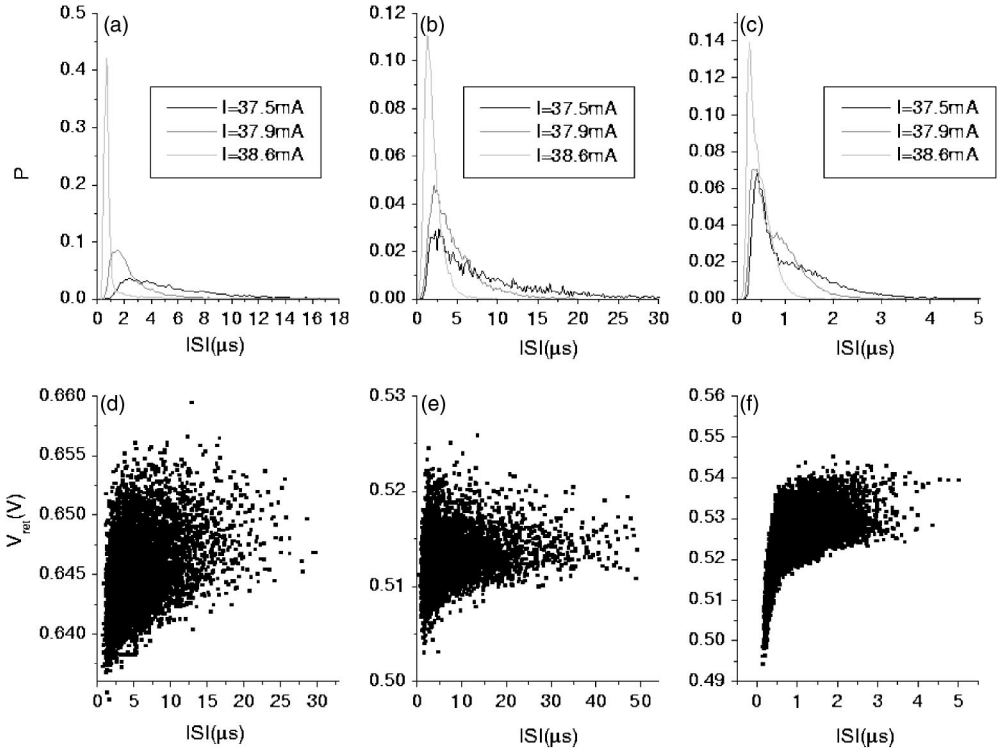

FIG. 10. Experimental dynamics with a destabilized MGM: Probability distribution of interdropout events (P) for different threshold reductions (a) $\xi=10.7\%$, (b) $\xi=9.3\%$, and (c) $\xi=8.8\%$. In each figure we show P for several values of pumping current (I) as is indicated in the insets. Map of the maximum point of return between two dropouts (V_{ret}) versus the time interval between them (ISI) for different threshold reductions: (d) $\xi=10.7\%$ and $I=37.63$ mA, (e) $\xi=9.3\%$ and $I=37.9$ mA, and (f) $\xi=8.8\%$ and $I=38.2$ mA.

best alignment condition to get rid of the MGM or inhibit its appearance in the main part of the experimental sweep. In this case, the same statistics were measured: the probability distribution of time between dropout events (P) and the coefficient of variation (CV). Leaving aside the case with the higher feedback [Fig. 6(c) with $\xi=10.7\%$], we observe that the statistics of this measurement is consistent with the dynamical model, if we compare a variation of the pumping current with a variation of the ϵ_1 parameter of the model [Fig. 6(c) and 10(a)–10(c) (this dependency of P in the pumping current has been previously obtained in Ref. [10] and in Ref. [28]). As previously observed Yacomotti *et al.* [10] the effect of reducing the feedback level on the probability distribution of time between dropout events is to increase the amplitude of the left peak approximately located at 0.5 μs, which is re-produced in this experiment [Figs. 10(a)–10(c). What is more, CV displays a zone in which its dependence on the threshold reduction is equivalent to the dependence that it has in the model on the ϵ_2 parameter. Moreover, this zone can be extended if the section of time series in which the laser is emitting in the MGM is discarded [Fig. 6(d), dotted line].

Also, the map of V_{ret} vs ISI reflects the similarity with the dynamical model. At $\xi=10.7\%$, the dynamics displayed is similar to the situation observed in the model at values far from the codimension-2 bifurcation point [Figs. 2(f) and 10(d)], whereas at $\xi=8.8\%$, it is similar to work near this point or even inside region I [Figs. 2(e) and 10(f)].

IV. CONCLUSIONS

We have shown that to obtain excitable behavior similar to the one observed in the model of Eguia *et al.* [9] it is necessary to get rid of the MGM. When the probability of appearance of the MGM is high, the dynamics can be separated into stable and bursting states [Figs. 5(a), 5(d), 8(a), and 8(b). As the feedback is reduced, the existence of two stable states, from which the dropouts are performed, becomes evident [Fig. 5(f), 8(c), and 8(d)].

Two limit cases were observed in the experimental condition of Sec. III A. When the feedback level is high the MGM is very stable, which causes a huge temporal dispersion between the burstinglike activity and the times between bursts. In other words, there exists a huge difference between the residence times in the MGM and the period of interburst time between dropouts (high CV values). Otherwise, when the feedback is reduced up to $\xi=6.8\%$ this temporal variability is also reduced (CV near 1), but the variability appears in the size of the dropouts (Fig. 9). This deteriorates the way in which the dropouts appear. Thus, it is impossible to distinguish a threshold because there are fluctuations of several amplitudes. Thus the high probability and stability of the MGM makes necessary to take the feedback level to a value in which the dropouts are badly formed, disabling its excitability.

ACKNOWLEDGMENTS

This work was partially funded by Fundación Antorchas, UBA, and CONICET.

[1] J. Risch and C. Voumard, J. Appl. Phys. **48**, 2083 (1977).
[2] M. Giudici, C. Green, G. Giacomelli, U. Nespolo, and J. R. Tredicce, Phys. Rev. E **55**, 6414 (1997).
[3] R. Lang and K. Kobayashi, IEEE J. Quantum Electron. **QE-16**, 347 (1980).
[4] T. Sano, Phys. Rev. A **50**, 2719 (1994).
[5] G. H. M. van Tartwijk, A. M. Levine, and D. Lenstra, IEEE J. Sel. Top. Quantum Electron. **1**, 466 (1995).
[6] J. Mulet and C. R. Mirasso, Phys. Rev. E **59**, 5400 (1999).
[7] G. Huyet, M. Giudici, C. Green, G. Giacomelli, and J. R. Tredicce, Opt. Commun. **149**, 341 (1997).
[8] G. Vaschenko, M. Giudici, J. J. Rocca, C. S. Menoni, J. R. Tredicce, and S. Balle, Phys. Rev. Lett. **81**, 5536 (1998).
[9] M. C. Eguia, G. B. Mindlin, and M. Giudici, Phys. Rev. E **58**, 2636 (1998).
[10] A. M. Yacomotti, M. C. Eguia, J. Aliaga, O. E. Martinez, G. B. Mindlin, and A. Lipsich, Phys. Rev. Lett. **83**, 292 (1999).
[11] G. Giacomelli, M. Giudici, S. Balle, and J. R. Tredicce, Phys. Rev. Lett. **84**, 3298 (2000).
[12] J. Hales, A. Zhukov, R. Roy, and M. I. Dykman, Phys. Rev. Lett. **85**, 78 (2000).
[13] Jorge M. Méndez, R. Laje, M. Giudici, J. Aliaga, and G. B. Mindlin, Phys. Rev. E **63**, 066218 (2001).
[14] F. Marino, M. Giudici, S. Barland, and S. Balle, Phys. Rev. Lett. **88**, 040601 (2002).
[15] Jorge M. Méndez, J. Aliaga, and G. B. Mindlin, Phys. Rev. Lett. **89**, 160601 (2002).
[16] J. C. Alexander, E. J. Doedel, and H. G. Othmer, SIAM (Soc. Ind. Appl. Math.) J. Appl. Math. **50**, 1373 (1990).
[17] M. A. Larotonda, A. Hnilo, J. M. Méndez, and A. M. Yacomotti, Phys. Rev. A **65**, 033812 (2002).
[18] H. J. Wünsche, O. Brox, M. Radziunas, and F. Henneberger, Phys. Rev. Lett. **88**, 023901 (2002).
[19] S. Barland, O. Piro, M. Giudici, J. R. Tredicce, and S. Balle, Phys. Rev. E **68**, 036209 (2003).
[20] C. Koch, *Biophysics of Computation: Information Processing in Single Neurons* (Oxford University Press, New York, 1999).
[21] M. C. Eguia, M. I. Rabinovich, and H. D. I. Abarbanel, Phys. Rev. E **62**, 7111 (2000).
[22] A. M. Yacomotti, G. B. Mindlin, M. Giudici, S. Balle, S. Barland, and J. Tredicce, Phys. Rev. E **66**, 036227 (2002).
[23] H. Kramers, Physica (Utrecht) **7**, 284 (1940).
[24] M. C. Eguia and G. B. Mindlin, Phys. Rev. E **61**, 6490 (2000).
[25] M. Timme, F. Wolf, and T. Geisel, Phys. Rev. Lett. **89**, 258701 (2002).
[26] A. Destexhe, M. Rudolph, J. M. Fellous, and T. J. Sejnowski, Neuroscience (Oxford) **107**, 13 (2001).
[27] T. Heil, I. Fischer, and W. Elsasser, Phys. Rev. A **58**, R2672 (1998).
[28] D. W. Sukow, J. R. Gardner, and D. J. Gauthier, Phys. Rev. A **56**, R3370 (1997).
[29] P. Hänggi, P. Talkner, and M. Borkovec, Rev. Mod. Phys. **62**, 251 (1990).